JACS
JOURNAL OF THE AMERICAN CHEMICAL SOCIETY

ARTICLE

pubs.acs.org/JACS

# Molecular Tunnel Junctions Based on $\pi$-Conjugated Oligoacene Thiols and Dithiols between Ag, Au, and Pt Contacts: Effect of Surface Linking Group and Metal Work Function

BongSoo Kim,[†,‡] Seong Ho Choi,[†] X.-Y. Zhu,[§] and C. Daniel Frisbie*[,†]

[†]Department of Chemistry and Department of Chemical Engineering and Materials Science, University of Minnesota, Minneapolis, Minnesota 55455, United States

[‡]Solar Cell Research Center, National Agenda Research Division, Korea Institute of Science and Technology (KIST), Seoul 136-791, Republic of Korea

[§]Department of Chemistry and Biochemistry, The University of Texas at Austin, 1 University Station, A5300 Austin, Texas 78712-0165, United States

Supporting Information

**ABSTRACT:** The tunneling resistance and electronic structure of metal−molecule−metal junctions based on oligoacene (benzene, naphthalene, anthracene, and tetracene) thiol and dithiol molecules were measured and correlated using conducting probe atomic force microscopy (CP-AFM) in conjunction with ultraviolet photoelectron spectroscopy (UPS). Nanoscopic tunnel junctions ($\sim$10 nm$^2$) were formed by contacting oligoacene self-assembled monolayers (SAMs) on flat Ag, Au, or Pt substrates with metalized AFM tips (Ag, Au, or Pt). The low bias (<0.2 V) junction resistance ($R$) increased exponentially with molecular length ($s$), i.e., $R = R_0 \exp(\beta s)$, where $R_0$ is the contact resistance and $\beta$ is the tunneling attenuation factor. The $R_0$ values for oligoacene dithiols were 2 orders of magnitude less than those of oligoacene thiols. Likewise, the $\beta$ value was 0.5 per ring (0.2 Å$^{-1}$) for the dithiol series and 1.0 per ring (0.5 Å$^{-1}$) for the monothiol series, demonstrating that $\beta$ is not simply a characteristic of the molecular backbone but is strongly affected by the number of chemical (metal−S) contacts. $R_0$ decreased strongly as the contact work function ($\Phi$) increased for both monothiol and dithiol junctions, whereas $\beta$ was independent of $\Phi$ within error. This divergent behavior was explained in terms of the metal−S bond dipoles and the electronic structure of the junction; namely, $\beta$ is independent of contact type because of weak Fermi level pinning (UPS revealed $E_F - E_{HOMO}$ varied only weakly with $\Phi$), but $R_0$ varies strongly with contact type because of the strong metal−S bond dipoles that are responsible for the Fermi level pinning. A previously published triple barrier model for molecular junctions was invoked to rationalize these results in which $R_0$ is determined by the contact barriers, which are proportional to the size of the interfacial bond dipoles, and $\beta$ is determined by the bridge barrier, $E_F - E_{HOMO}$. Current−voltage ($I$−$V$) characteristics obtained over a larger voltage range 0−1 V revealed a characteristic transition voltage $V_{trans}$ at which the current increased more sharply with voltage. $V_{trans}$ values were generally >0.5 V and were well correlated with the bridge barrier $E_F - E_{HOMO}$. Overall, the combination of electronic structure determination by UPS with length- and work function-dependent transport measurements provides a remarkably comprehensive picture of tunneling transport in molecular junctions based on oligoacenes.

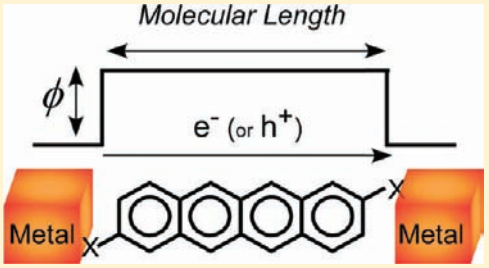


## INTRODUCTION

Understanding the role of metal−molecule contacts in molecular electronics experiments remains a major challenge.[1−12] In a typical molecular junction, a molecule or an ensemble of molecules is contacted at either end by metal electrodes, Figure 1. The goal is to understand the current−voltage ($I$−$V$) characteristics in terms of the molecular structure and the type of chemical linking groups (X) employed to connect the molecules to the electrodes. However, in these two-terminal measurements one does not have independent knowledge of the potential profile across the junction, and thus the relative contribution of the contacts to the junction $I$−$V$ characteristic (or total resistance) is generally unknown.

Because the role of the contacts cannot be discerned by $I$−$V$ measurements on any single molecular junction, systematic examination of contact effects are required in which the nature of the contact is changed, e.g., by switching the type of linking groups, or by measuring the dependence of the $I$−$V$ characteristics on molecular length. The length dependence approach that we[7,8,13,14] and others[10,15−18] have emphasized is preferable because it can be quantitative: from plots of differential resistance (at a given voltage) versus molecular length the effective contact resistance can be extrapolated. For example, in the nonresonant tunneling regime the junction resistance follows,

$$R = R_0 \exp(\beta s) \quad (1)$$

**Received:** August 16, 2011
**Published:** October 21, 2011

  

where $R_0$ is the contact resistance, $s$ is the molecular length (or barrier thickness), and $\beta$ is the tunneling attenuation factor that depends on the average barrier height. Plots of log $R$ versus $s$ yield estimates of $\beta$ from the slope and $R_0$ from the zero length intercept. Thus, length-dependent transport measurements decouple the contacts from the "bulk" transport through the molecule, and comparison of $R_0$ values for different junctions clearly indicates the relative roles of the contact resistance.[19]

We have shown previously with conducting probe atomic force microscopy (CP-AFM) that length-dependent measurements can determine contact resistances in alkane thiol and dithiol junctions as a function of the metal work function.[7,13] These measurements revealed a very strong dependence of $R_0$ on metal type for alkane monothiols; the contact resistance varied by 4 orders of magnitude as the work function changed from 4.3 (Ag contacts) to 5.7 eV (Pt contacts). $\beta$ was found to be independent of the work function. In addition, these measurements confirmed prior reports[2] that chemical contacts (Au−S bonds) have significantly lower resistance than physical contacts (e.g., Au/$CH_3$). The CP-AFM technique is ideal for such experiments because junctions are readily formed by soft contact of the tip to well-characterized self-assembled monolayers (SAMs), and the contact work function can be changed easily by using tips and substrates coated with different metals.

Here, we expand these earlier experiments to rigid, $\pi$-conjugated, thiol- and dithiol-capped oligoacenes ranging from one to four aromatic rings (0.8−1.5 nm) in length, Figure 2. Such $\pi$-conjugated oligoacene systems have been examined previously[8,20−22] but not as a systematic function of length up to four acene rings as reported here. The tetracene mono- and dithiol molecules are the longest oligoacenes to be probed in a molecular junction. In general, the oligoacenes are a good model system for molecular electronics because they are rigid, planar, and aromatic.

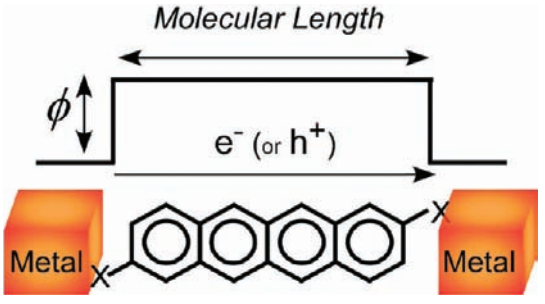


**Figure 1.** Schematic representation of charge transport in metal−molecule−metal junctions. Charge carriers (electrons or holes) tunnel through a barrier ($\phi$) with width equal to the molecular length. X represents a surface linking group used to bind the molecule to the metal.

We initiated these studies with a systematic investigation of the electronic structure of oligoacene SAMs on Ag, Au, and Pt by ultraviolet photoelectron spectroscopy (UPS). Very few molecular junction transport experiments have been correlated with experimentally determined electronic structure, and the possibility of such a correlation with junctions based on SAMs is an advantage for developing a comprehensive picture of the junction behavior.[7,23,24] We find by UPS that the Fermi level $E_F$, or more specifically the Fermi level to HOMO level offset ($E_F - E_{HOMO}$), is weakly pinned in these oligoacene systems, i.e., it does not depend strongly on metal work function $\Phi$ (Ag to Au to Pt) because of the presence of a large bond dipole associated with the metal−S contact. The origin of the bond dipole is electron donation from S to the metal, and it increases with increasing $\Phi$, as expected, which then mitigates the variation of $E_F - E_{HOMO}$ with $\Phi$. Further, the bond dipole results in a change in the metal work function $\Delta\Phi$ that clearly impacts the junction transport characteristics. In particular, there is excellent correlation between $\Delta\Phi$ and $R_0$ for Ag, Au, and Pt contacts to oligoacene thiol SAMs. We also find that the other key tunneling parameter, $\beta$, is essentially independent of $\Phi$ and $\Delta\Phi$ within error. The divergent dependences of $\beta$ and $R_0$ on the metal type can be explained self-consistently with a multibarrier model for the junction based on prior theoretical work by Heimel et al.[25,26] In this model, contact barriers are present at the interfaces between the molecules and the metals due to the metal−S bond dipoles. The two contact barriers are proportional to $\Delta\Phi$, and we propose that $R_0$ reflects these barriers. The bridge barrier, which is associated with the oligoacene backbone and impacts $\beta$, is determined by $E_F - E_{HOMO}$ and is only weakly sensitive to the work function of the metals because of the pinning effect.

As expected based on earlier results,[2,7,9] we also find that the resistance of metal−oligoacene−metal junctions depends strongly on whether monothiol or dithiol molecules are employed, i.e., junctions with two "chemical contacts" have dramatically lowered junction resistances compared with junctions with one chemical contact and one physical contact (this is independent of the specific metal). Surprisingly, however, the lower junction resistance for dithiols reflects differences in both $R_0$ and $\beta$, a point that is only clear when the length dependence of transport is systematically examined. That is, $\beta$ (not just $R_0$) is lower for oligoacene dithiol junctions than for oligoacene monothiol junctions, highlighting the key role that contacts play

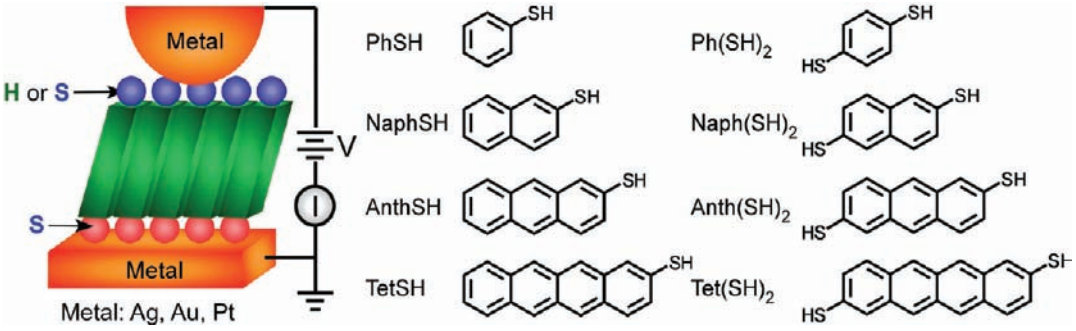


**Figure 2.** Schematic representation of a CP-AFM junction on the left. A metal-coated (Ag, Au, or Pt) AFM tip is brought into contact with a SAM of $\pi$-conjugated oligoacene thiols or dithiols of various lengths on a metal substrate at a load of 1 nN. Voltage is swept at the tip, and current−voltage characteristics are recorded. The molecular structures are shown on the right.

in junction transport properties. We propose that in the case of dithiol junctions, the HOMO level is weakly pinned closer to $E_F$ than in the case of monothiol junctions.

Collectively, these results provide a comprehensive picture of tunneling transport in oligoacene junctions in which the roles of the surface linkers and metal work functions on both $R_0$ and $\beta$ are clearly delineated. The tunneling characteristics of conjugated oligoacenes are profoundly affected by the contacts, confirming theoretical predictions[24,25] and reinforcing the conclusion that interpretation of junction $I-V$ characteristics requires careful consideration of contact properties. We emphasize that both photoelectron spectroscopy and length-dependent transport measurements are critical for the overall analysis of contact effects, and we believe that, in broad terms, the results we present here are likely to be similar for junctions based on other short conjugated molecules.[24,27−31]

## EXPERIMENTAL SECTION

**Materials.** Synthesis of oligoacene thiols and dithiols in Figure 2 except benzenethiol (PhSH) and naphthalene-2-thiol (NaphSH) are provided in Supporting Information. PhSH, NaphSH, and the other chemicals used for the synthesis were purchased from Aldrich. Tetrahydrofuran (THF) and triethylamine (TEA) were dried following procedures in the literature.[32] Gold nuggets (99.999% pure) were purchased from Mowrey, Inc. (St. Paul, MN). Evaporation boats and chromium evaporation rods were purchased from R. D. Mathis (Long Beach, CA). Platinum and titanium for e-beam evaporation were purchased from Kamis, Inc. (Mahopac Falls, NY). Silicon (100) wafers were obtained from WaferNet (San Jose, CA). Contact mode AFM tips (DNP silicon nitride probes) were obtained from Veeco Instruments (Camarillo, CA). Absolute ethanol was purchased from Fisher Scientific.

**Monolayer Growth and Characterization.** The Ag or Au substrates were 1000 Å thick thin films on silicon (with a 50 Å Cr adhesion layer) prepared in a Balzers thermal evaporator at a rate of 1.0 Å/s at a base pressure of $\leq 2 \times 10^{-6}$ Torr. The Pt substrates were 1000 Å films on silicon prepared in an e-beam evaporator (SEC 600) with a 50 Å Ti adhesion layer. The metal surfaces were immersed in 10 mL of 0.01−0.1 mM solutions of the thiol molecule in argon-purged absolute ethanol. SAMs of PhSH, NaphSH, and AnthSH were grown for 18−24 h. For the preparation of SAMs of tetracene thiol, we added 30 $\mu$L of triethylamine (TEA) to the tetracene-2-thioacetate (TetSAc) solution for deprotection of acetyl group and SAM growth on Ag substrates (36 h) or 10 $\mu$L of concentrated aqueous ammonia solution for SAM growth on Au and Pt substrates (24 h). Note that for some reason (presumably partial oxidation of the Ag surfaces that were briefly air-exposed before immersion in ethanol), quality SAM formation on Ag substrates required longer immersion times. When the SAM growth conditions for Au and Pt were applied, the SAM thickness on Ag substrates was lower than expected. Therefore, we added more triethylamine deprotecting agent and immersed Ag substrates for longer times.

In the case of dithiol molecules, 30 $\mu$L of TEA was added to the solution of the acetyl-capped molecules for deprotection and SAM growth (18−24 h), following a published procedure.[33] After removing the samples from the solutions and rinsing with toluene and ethanol, we reimmersed each sample in 10 mL of pure absolute ethanol with 20 $\mu$L of TEA or concentrated aqueous ammonia solution for another 24 h to ensure the complete removal of acetyl groups on the outer terminus of the SAMs. All SAM samples were rinsed thoroughly with toluene and ethanol and stored in argon-purged absolute ethanol for less than 12 h and dried under a stream of $N_2$ before all measurements.

We characterized the SAMs using spectroscopic ellipsometry and XPS. Ellipsometry measurements were carried out on a VASE spectroscopic ellipsometer (J. A. Woolam Co., Inc.). Measurements of the polarization angles ($\Psi$ and $\Delta$) were taken as a function of wavelength ($\lambda$) between 600 and 1000 nm at an incident angle of 65°. The indices of refraction ($n(\lambda)$) and extinction coefficients ($k(\lambda)$) of the metal-coated substrates were determined by measurement of the polarization angles prior to monolayer deposition. The instrument software converted these values to $n(\lambda)$ and $k(\lambda)$ of metal films and saved them as a material file. After monolayer formation on metal substrates, the polarization angles were measured again and the film thicknesses were determined by a built-in algorithm. $n(\lambda)$ and $k(\lambda)$ of the SAMs were assumed to be 1.55 and 0, respectively, over the wavelength range.

We acquired XPS spectra on a Perkin-Elmer Phi 5400 spectrometer. The Mg $K_\alpha$ X-ray (1253.6 eV) anode was operated at 200 W. Photoelectron detection was accomplished with a hemispherical analyzer set at a pass energy of 89.45 eV for survey scans and 17.9 eV for high-resolution scans. Each sample was transferred into the ultrahigh vacuum chamber immediately after drying under a stream of nitrogen to minimize contamination or oxidation. To obtain monolayer thicknesses, we carried out XPS measurements on SAMs of alkanethiols ($CH_3(CH_2)_nSH$, $n$ = 7, 9, 11, 13, 15) on each metal and obtained calibration curves for the relative peak areas of the metal (Ag $3d_{5/2}$, Au $4f_{7/2}$, or Pt $4f_{7/2}$) and the C 1s peaks, using known thicknesses of these SAMs from the literature.[34,35] These calibration curves were used to obtain the thicknesses of the oligoacene thiol SAMs. Additional description of the characterization of the monolayers is provided in Figures S1 and S2 and Tables S1 and S2 in Supporting Information.

**Determination of Molecular Energy Levels.** To probe the electronic structure of the SAMs on metals (Ag, Au, and Pt), we acquired UPS spectra on a Perkin-Elmer Phi-5400 spectrometer equipped with a He I ($h\nu$ = 21.2 eV) radiation source at an incident angle of 50° from the sample normal. Photoemitted electrons were collected at normal emission with a pass energy of 4.45 eV. All spectra were acquired at an applied bias of −7 V on the sample, and the energy scale was referenced to the metal Fermi level ($E_F$). The intensities of the raw spectra were normalized at $E_F$. The onsets of the highest occupied molecular orbitals were determined from the UPS spectra. After magnifying the first increasing peak near the metal Fermi level, we found the onset point from the cross-point between two trend lines (one is placed on the baseline and the other on the slope of the first peak, see Supporting Information). Optical gaps were determined from the onset of UV−visible absorption spectra using a procedure similar to the determinations of UPS onsets. The optical gap corresponds to the lowest gap between the lowest occupied molecular orbital band and the highest occupied molecular orbitals. UV−visible absorption spectra were obtained on a Hewlett-Packard 8453 UV−vis spectrophotometer from chloroform solutions of PhSH, NaphSH, AnthSH, and acetyl protected molecules (in place of TetSH and dithiols) at a concentration of $\sim 10^{-5}$ M (the maximum absorbance was ~1).

**Preparation of Metal-Coated AFM Tips and Flat Metal Substrates.** For Ag and Au tips, contact mode AFM tips were coated with 250 Å Ag or Au on top of a 30 Å Cr adhesion layer using a metal evaporator inside a glovebox and transferred without exposing to air to another glovebox where electrical measurements were carried out. For Pt tips, contact mode AFM tips were coated with an 80 Å Pt film on top of a 30 Å Ti adhesion layer using an e-beam evaporator, and then immediately transferred to the measurement glovebox with ~10 min air exposure. Template-stripped flat metal substrates were used to grow monolayers for reproducible electrical measurements.[7,8] Flat metal substrates were prepared by the following steps. For flat Ag or Au substrates, 5000 Å of Ag or Au was first deposited onto clean Si wafers in an e-beam evaporator. We then glued Si chips (0.5 cm ×0.5 cm) onto the metal surface using epoxy (EPO-TEK 377, Epoxy Technologies, MA). The epoxy layer was cured by placing the wafers in an oven at 120 °C for 1 h. The flat metal substrates were peeled off from the silicon surface and immersed immediately in the thiol or dithiol solution for

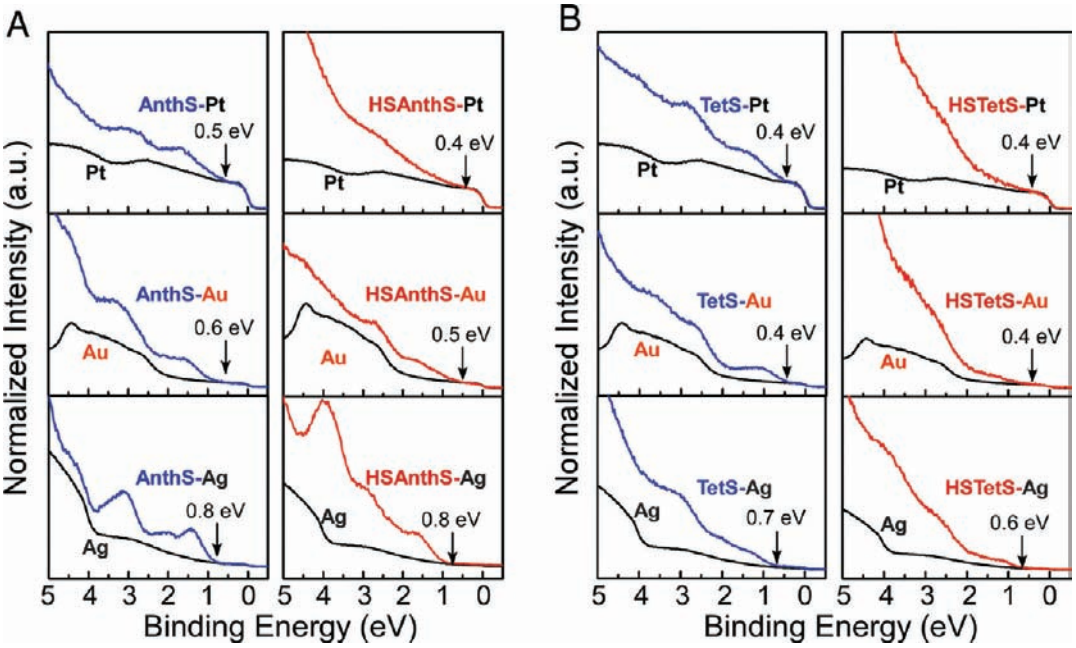


**Figure 3.** UPS spectra of (A) AnthSH and Anth$(SH)_2$ and (B) TetSH and Tet$(SH)_2$ on Ag, Au, and Pt. Binding energies are referenced to the Fermi level, $E_F$. Arrows indicate the onsets of the HOMOs. The spectral intensity of SAM-coated metal substrates was normalized to the intensity of bare metal substrates at 0 eV. "—" represents chemical contact to metal.

SAM growth. For flat Pt substrates, 3000 Å of Pt was sputter-coated onto a clean Si wafer in a Perkin-Elmer 2400 DC sputterer at a rate of ~3 Å/s. On top of the Pt film, subsequent depositions of 300 Å of Cr and 2000 Å of Au were carried out in a thermal evaporator. Note that the Cr layer prevented the penetration of Au atoms into the Pt film. The Au film enhanced the yield of flat Pt substrates due to better adhesion with the cured epoxy layer. The rest of the steps were the same as for flat Ag or Au substrates.

**Current−Voltage (*I*−*V*) Measurements.** We formed the junctions by contacting a SAM on flat Ag, Au, or Pt substrates with a Ag-, Au-, or Pt-coated AFM tip at a load of 1 nN using a Veeco (Digital Instruments) Multimode AFM in a glovebox ($O_2$ < 7 ppm), as illustrated in Figure 2.[7,8] Current−voltage measurements were carried out using a Keithley model 236 electrometer with a DC voltage applied to the AFM tip as controlled with LabVIEW software. For the length dependence experiments, each metal−molecule−metal junction was examined over a voltage range of ±0.2 V. Ten to twenty *I*−*V* traces were collected for each molecular junction. A tip radius of ~50 nm was used in all experiments, and in our previous work[13,36,37] the corresponding contact area was estimated to be on the order of 25 $nm^2$, which would correspond to roughly 100 molecules in the contact. Linear fits to each *I*−*V* trace yielded low-bias (within ±0.2 V) resistances that were then averaged for each molecule. Extrapolation of this low-bias average resistance versus the number of benzene rings to zero rings gave the contact resistance ($R_0$). The slope of the resistance versus length plot gave the $\beta$ value. For larger voltage sweeps (up to ±0.8−1 V), 10−20 *I*−*V* traces were collected and averaged for each SAM.

In general, measurements on oligoacene dithiol junctions were more difficult than on monothiol junctions because of sudden tip degradation. 'Degradation' means that tips suddenly showed extremely low currents after normal behavior. Tip degradation was probably due to either (i) ohmic heating which disrupted or fractured the tip metal coating, (ii) contamination of the tip by bonding and extraction of molecules from the dithiol SAM, or (iii) mechanical failure (peeling) of the tip metal film when the tip was retracted from the surface. To facilitate the dithiol measurements, several tips were employed to complete the length dependence series. The tips were calibrated with respect to an octanethiol SAM reference sample; only tips that gave the same resistance ($6.2 \times 10^7$ Ω) within 5% were used for the dithiol oligoacene measurements. Moreover, tips were always checked by comparing resistances on the same oligoacene dithiol before moving to other oligoacene samples. Averaging of the *I*−*V* data was accomplished in the same manner as described above.

## RESULTS AND DISCUSSION

**Energy Level Alignment.** Electronic structures of the oligoacene SAMs were probed by UV−visible absorption spectroscopy and UPS spectroscopy. UV−visible absorption spectra (Figure S5, Supporting Information) reveal that as the number of benzene rings increases, the HOMO−LUMO gaps decrease linearly from 4.0 to 2.5 eV because of efficient conjugation in the planar aromatic structure. We determined the HOMO levels with respect to the metal Fermi level ($E_F$) from the onset of photoemission. Figure 3 displays the UPS spectra for SAMs of AnthSH, Anth$(SH)_2$, TetSH, and Tet$(SH)_2$ on Ag, Au, and Pt surfaces (see Figure S3 in Supporting Information for details illustrating how we determined the HOMO onset and work function from UPS spectra). The HOMO levels ($E_{HOMO,onset}$) of all oligoacenes are compiled in Table 1. As expected, the $E_{HOMO,onset}$ levels move closer to $E_F$ as molecular length increases.[38] Moreover, for the oligoacene dithiols, the HOMO bands lie slightly closer to $E_F$ than for the corresponding monothiol molecular bands, and peaks for dithiol monolayers appear broader than those of monothiol monolayers. The peak broadening could have several origins: (i) different intrinsic characteristics, i.e., different molecular orbital mixing between metal−oligoacene monothiol and metal−oligoacenedithiol; (ii) somewhat lower quality of the dithiol monolayer because part of the dithiol molecules are lying down (see Table S2 in Supporting

**Table 1. Summary of $E_F - E_{HOMO,onset}$ Values and Modified Metal Work Function Obtained from UPS Spectra (unit: eV)[a]**

| | | | | film work function | | | | | |
|---|---|---|---|---|---|---|---|---|---|
| | $E_F - E_{HOMO,onset}$ | | | Ag (4.26) | | Au (5.20) | | Pt (5.65) | |
| molecule | Ag | Au | Pt | $\Phi_{SAM}$ | $\Delta\Phi$ | $\Phi_{SAM}$ | $\Delta\Phi$ | $\Phi_{SAM}$ | $\Delta\Phi$ |
| PhSH | 1.2 | 1.1 | 0.8 | 3.9 | −0.4 | 4.4 | −0.8 | 4.0 | −1.7 |
| NaphSH | 1.1 | 0.9 | 0.6 | 4.0 | −0.3 | 4.4 | −0.8 | 4.0 | −1.7 |
| AnthSH | 0.8 | 0.6 | 0.5 | 3.9 | −0.4 | 4.2 | −1.0 | 4.1 | −1.6 |
| TetSH | 0.7 | 0.4 | 0.4 | 3.9 | −0.4 | 4.1 | −1.1 | 4.1 | −1.6 |
| $Ph(SH)_2$ | 1.1 | 0.9 | 0.8 | 3.8 | −0.5 | 4.3 | −0.9 | 4.5 | −1.2 |
| $Naph(SH)_2$ | 0.9 | 0.6 | 0.5 | 4.0 | −0.3 | 4.1 | −1.1 | 4.3 | −1.4 |
| $Anth(SH)_2$ | 0.8 | 0.5 | 0.5 | 4.1 | −0.2 | 4.3 | −0.9 | 4.2 | −1.5 |
| $Tet(SH)_2$ | 0.6 | 0.4 | 0.4 | 4.1 | −0.2 | 4.0 | −1.2 | 4.2 | −1.5 |

[a] Experimental errors are approximately ±0.1 eV.

Information); (iii) inhomogeneous molecular environments and intermolecular coupling.[39]

It is also evident from the photoemission cutoff regime of the UPS spectra (shown in Figures S3 and S4) that there is a substantial work function change ($\Delta\Phi = \Phi_{SAM} - \Phi$) for the metals due to the presence of the adsorbed SAMs. Here $\Phi$ represents the original metal work function, and $\Phi_{SAM}$ is the work function of the SAM-coated metal. The values of $\Phi$, $\Phi_{SAM}$, and the work function changes, $\Delta\Phi$, are reported in Table 1, where it is clear that there is very weak dependence of both $\Phi_{SAM}$ and $\Delta\Phi$ on oligoacene length or the presence/absence of a terminal SH group. However, $\Delta\Phi$ does depend strongly on metal type: $\Delta\Phi$ is −0.3 (±0.1), −1.0 (±0.1), −1.5 (±0.2) eV for Ag, Au, and Pt, respectively. $\Delta\Phi$ substantially reduces the intrinsic metal work function difference for the SAMs; the HOMO levels of the oligocenes are ultimately lying relatively close to each other on different metal substrates (see $E_F - E_{HOMO,onset}$ in Table 1). For a given oligoacene length, the $E_F - E_{HOMO,onset}$ values are quite similar, especially when considering the large variation in the work functions of the unmodified metals: Ag (4.26 eV), Au (5.20 eV), and Pt (5.65 eV).

Work function changes for SAMs on metals have been investigated extensively experimentally[38,40,41] and theoretically.[25,26,42,43] Conceptually, work function changes for metal surfaces with oriented, adsorbed molecules are considered to be the sum of three interfacial dipoles: (i) the intrinsic molecular dipole, (ii) the intrinsic metal dipole that changes upon adsorption (i.e., the surface electron "push-back" effect);[40,41] (iii) the metal−linker (e.g., metal−S) bond dipole. Recent density functional theory (DFT) calculations have delineated the local charge redistribution at metal/SAM interfaces that gives rise to the bond dipole (BD).[25,26,42,43] Using DFT, Heimel et al. have shown that upon adsorption of aromatic thiolate to various metals, electron density in the C(aromatic ring)−S bond decreases while that of the S−metal bond increases, i.e., there is a net electron donation to the metal.[25,26] The same computations reveal that the magnitudes of the BDs for thiol linkages depend strongly on the metal type, namely the BD increases as the work function increases. Furthermore, the BD can result in large electrostatic potential changes (0−1 eV) across only a few Å distance associated with metal−S−C(aromatic ring) linkages. The creation of such bond dipoles in turn mitigates the variation of $E_F - E_{HOMO}$ with $\Phi$ for aromatic SAMs, resulting in partial pinning of the molecular HOMO levels with respect to the Fermi level $E_F$.[25,26,43] These calculations are consistent with our results (see below) and prior UPS work by others.[38,40,41] Therefore, we believe it is likely that the metal−S BD is mainly responsible for $\Delta\Phi$ and that the BD depends strongly on metal type (Ag < Au < Pt).

Figure 4 summarizes our findings concerning energy level alignment for oligoacene molecules on Ag, Au, and Pt based on the UPS and UV−visible data. Figure 4A is a scheme of the vacuum level shift due to $\Delta\Phi$ and the work function $\Phi_{SAM}$ for the three different metals. Figure 4B shows the HOMO and LUMO levels of all oligoacene SAMs with respect to $E_F$. The LUMO levels are constructed from the optical HOMO−LUMO gaps, assuming that the optical gaps of the SAMs are the same as those of the molecules in solution and independent of the metal substrate.[44−46] (Note that the LUMO positions are underestimated by the exciton binding energy, 0.5−1.0 eV.[46]) From the estimated energy level alignment in Figure 4B, it is evident that the HOMO levels lie much closer to $E_F$, which indicates that the HOMO plays an important role in facilitating tunneling in junctions based on all of the oligoacenes. Of course, these energy level diagrams based on UPS and UV−visible data do not account for the influence of the second metal contact on the electronic structure; these diagrams are for single SAM-coated metal interfaces. It is likely that the effect of a second metal contact in a junction would be to position the HOMO band even closer to $E_F$, as reported in previous studies.[47−51] This is because one expects that strong coupling between the molecular orbitals and the second metal due to the metal−S bonds would further broaden the frontier orbitals, resulting in a decrease in $E_F - E_{HOMO}$ for the full junction.[52−55] Note that this view presumes that HOMO level broadening in a dithiol junction overrides any effect of a second bond dipole at the second contact; i.e., the orientation of the metal−S bond dipoles is such that one might conclude that a second metal−S bond would actually *increase* $E_F - E_{HOMO}$. This does not appear to happen (based on transport data below), and understanding the detailed reason for this will probably require further calculations.

Figure 4 shows clearly that for a given oligoacene length the HOMO level position, $E_F - E_{HOMO}$ does not vary with metal type as much as one might expect based on the 1.4 eV span in work functions of the unmodified metals (Ag to Pt). This point is quantified in Figure 5A which displays $E_F - E_{HOMO}$ versus $\Phi$ for the oligoacene monothiols on Ag, Au, and Pt. The linear fit to the anthracene thiol data reveals that while $E_F - E_{HOMO}$ is correlated with $\Phi$, the dependence is weak (slope = −0.22), indicating weak pinning of the HOMO level with respect to the metal. On the other hand, as expected, $E_F - E_{HOMO}$ does depend on the length of the oligoacene, as shown in both Figure 5A and 5B.

The correlation of $\Delta\Phi$ with $\Phi$ and molecular length, Figure 5C and 5D, is important for our later discussion. Figure 5C reveals that $\Delta\Phi$ trends linearly with $\Phi$, with a slope of −0.86 and a correlation coefficient $R^2 = 0.89$ for the linear fit to the monothiol data. The interpretation is that the magnitude of the metal−S BD scales almost one-to-one with $\Phi$, becoming very large for the Pt−S bond. In contrast, $\Delta\Phi$ has almost no dependence on molecular length, Figure 5D, which is consistent with the interpretation that $\Delta\Phi$ originates primarily from the metal−S BD, and that therefore $\Delta\Phi$ represents a very localized barrier height change, essentially within the metal−S contact; this is a point to which we will return.

**General *I*−*V* Behavior.** We turn now to the transport data. Figure 6 displays representative *I*−*V* characteristics of Au−oligoacene

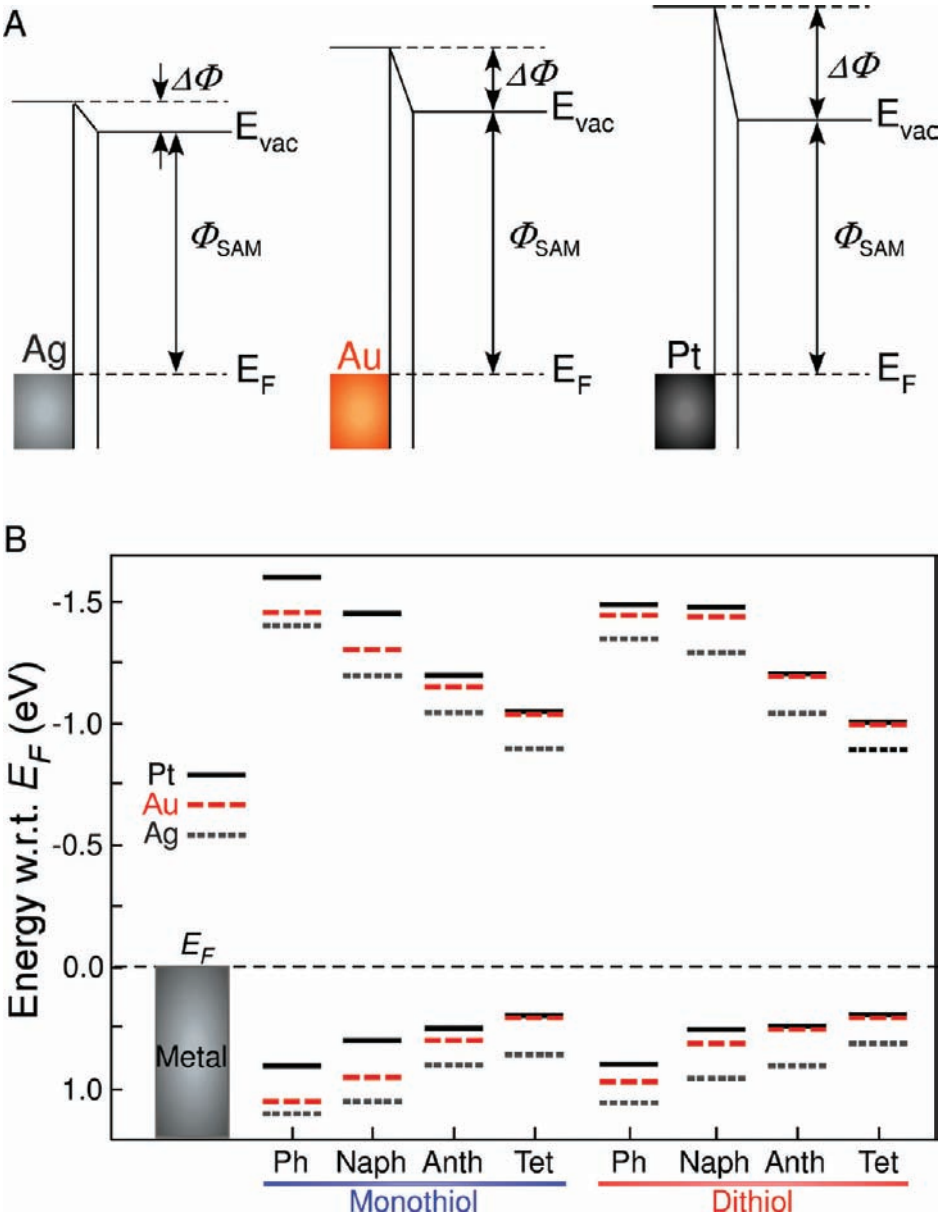


**Figure 4.** Estimated vacuum level change (A) and HOMO/LUMO alignment with respect to $E_F$ (B) of oligoacene thiols and dithiols for Ag, Au, and Pt surfaces (the data from Table 1 and Figure S5). In panel A, $\Delta\Phi$ stands for the work function change, $\Phi_{SAM}$ for the work function of SAM-coated metals, $E_F$ for the metal Fermi level, and $E_{vac}$ for the vacuum level. In panel B, the LUMO levels are constructed from the optical HOMO−LUMO gaps.

thiol−Au and Au−oligoacene dithiol−Au junctions. Each $I-V$ trace has a sigmoidal shape and is nearly symmetric with respect to zero bias. For a given voltage, the current decreases exponentially with length. These attributes indicate that nonresonant tunneling is the principal transport mechanism at low bias in these junctions.[56,57] Detailed analysis and discussion of both the low and high voltage transport regimes follow below.

**Low Bias Junction Characteristics.** We have examined the molecular length dependence of the junction resistance in the low bias regime (±0.2 V). Figure 7 displays a semilog plot of resistance versus number of rings for oligoacene thiol and dithiol junctions. Each data point reflects the average of 10−20 $I-V$ traces. Note that we were not able to acquire good data for Ag−oligoacene dithiol−Ag junctions because of junction instability. This is perhaps because Ag atoms are liable to electromigration under bias.[58,59] The linear relationships in Figure 7 indicate that the data are well explained by nonresonant tunneling (see eq 1), with an average $\beta$ value determined from the slopes of the semilog plots of 1.0 ± 0.13 per ring or 0.5 Å$^{-1}$ for monothiols and 0.5 ± 0.07 per ring or 0.2 Å$^{-1}$ for dithiols.

The $\beta$ value in the dithiol junctions is consistent with previous reports on tunneling in aromatic dithiols and diamines.[18,60−62] However, the difference in $\beta$ between monothiols and dithiols with the same conjugated backbone has not been reported previously ($\beta$ values for alkane thiols and dithiols are the same[7]). This difference is perhaps surprising given that the molecular backbone structures are identical, and it implies that $E_F - E_{HOMO}$ offsets for dithiols are lower than for monothiols.[63] The HOMO level alignments measured by UPS for the two types of SAMs are not very different, however (the difference of

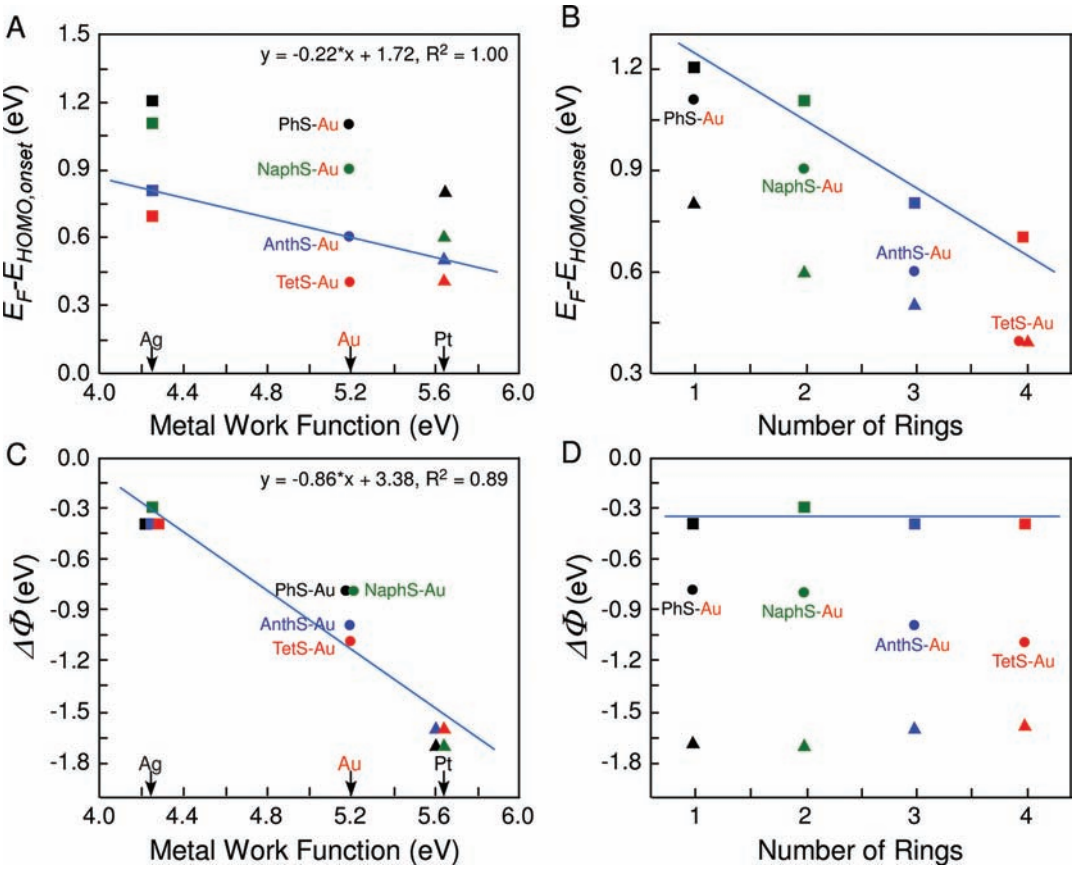


**Figure 5.** Correlations of the data shown in Table 1. (A) Plot of $E_F - E_{HOMO,onset}$ versus metal work function $\Phi$. (B) Plot of $E_F - E_{HOMO,onset}$ versus number of rings. (C) Plot of work function change $\Delta\Phi$ versus metal work function $\Phi$. (D) Plot of work function change $\Delta\Phi$ versus number of rings. Symbols for metals: Ag (square), Au (circle), and Pt (triangle) and colors for molecules: PhSH (black), NaphSH (green), AnthSH (blue), and TetSH (red). Blue lines are linear least-squares fits in plots A and C and guides for the eye in plots B and D.

$E_F - E_{HOMO,onset}$ values between monothiol and corresponding dithiol SAMs is approximately 0−0.2 eV, see Table 1). Yet here it is important to note that the $E_F - E_{HOMO}$ offsets measured by UPS do not reveal the actual offsets in completed junctions with two contacts. That is, the scheme in Figure 4 likely does not capture the electronic role played by the second contact in a fully assembled junction. This conclusion is consistent with many previous studies in which the tunneling barrier in alkanethiol junctions has been estimated to be much lower than the spectroscopic $E_F - E_{HOMO}$ offset.[7,27,40,64] It is reasonable to expect that for junctions based on dithiol molecules the tunneling barriers will be significantly smaller than the barriers for monothiols, because there is likely significant electronic broadening of the HOMO level in junctions with two chemical contacts.[51,52,64] The lower $\beta$ values for dithiols reflect the lower barriers and highlight the key role of chemical contacts; two chemical contacts in the oligoacene dithiol junctions create a smaller tunneling barrier through the oligoacene backbone.

Figure 7 also indicates that the $\beta$ values for both mono- and dithiols, respectively, appear to be independent of metal work function within experimental uncertainty. The results of multiple measurements of $\beta$ versus work function are summarized in Figure 8A, and indeed there appears to be no systematic trend. We conclude then that the average tunneling barrier height is strongly dependent on the number of chemical contacts (1 vs 2) but not on metal type. The lack of dependence of $\beta$ on $\Phi$ is a central result of this work, and it is consistent with our finding that $E_F$ is weakly pinned in these systems, i.e., that the effective tunneling barrier is *approximately* the same for all monothiol junctions and for all dithiol junctions, respectively (see Figure 4B). We will return to this below in the context of describing the nature of the tunneling barrier.

We can also conclude from Figure 7 that the precise values of the metal−S−C bond angles, which can be different for the Ag, Au, and Pt substrates,[65] are not critical for $\beta$, as it is clear that the slope of the resistance vs length data are independent of the contact type. This result is consistent with "through-bond tunneling" and previous reports.[24,37]

The junction contact resistances $R_0$ can be determined from the $y$-intercepts of the plots in Figure 7. All $R_0$ values are displayed as a function of unmodified metal work function ($\Phi$) in Figure 8B. There are three important observations associated with Figure 8B: (i) $R_0$ decreases strongly with increasing metal work function; (ii) dithiol contacts have much lower $R_0$ than monothiol contacts for a given set of metal electrodes; (iii) molecular junctions incorporating a pair of mixed metal electrodes (e.g., Ag tip/Au substrate and Au tip/Ag substrate) have $R_0$ values that are positioned between the $R_0$s for the homometal junctions (e.g., Ag tip/Ag substrate and Au tip/Au substrate).

These observations are consistent with our previous report on work function effects in junctions incorporating alkane thiols and dithiols[7] and with the work of others on mono- versus

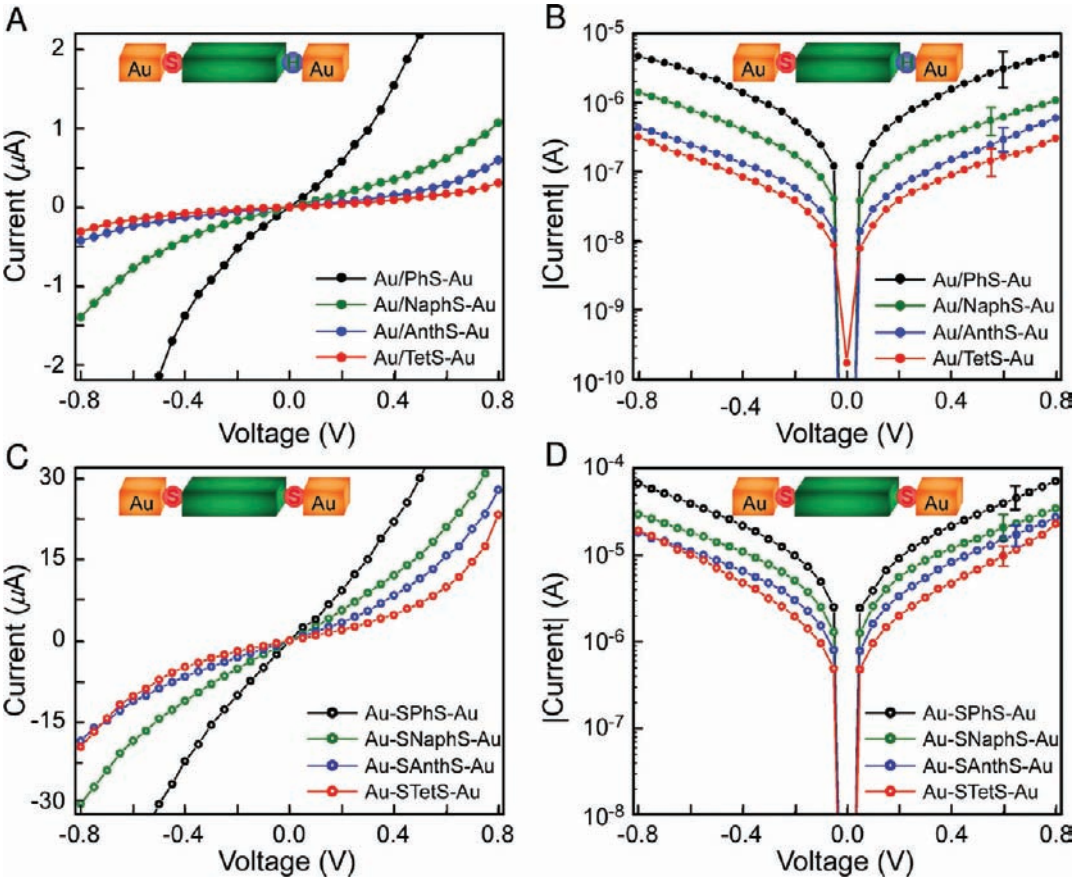


**Figure 6.** Representative linear and semilog plots of average $I-V$ traces of Au−oligoacene thiol−Au (A, B) and Au−oligoacene dithiol−Au junctions (C, D). Error bars in plots B and D are given at a single point near 0.6 V for clarity.

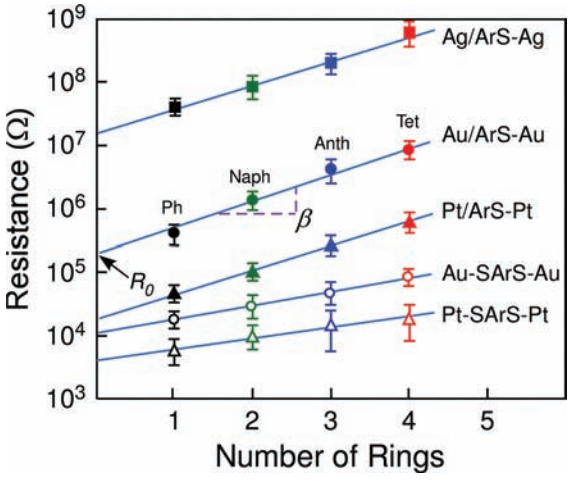


**Figure 7.** Semilog plot of resistance versus number of rings for oligoacene thiol and dithiol junctions. Resistances were calculated from the average of 10−20 $I-V$ traces within ±0.2 V. The error bars represent one standard deviation from the mean. "−" represents chemical contact to metal and "/" represents physical contact.

dithiols.[16,17] Indeed, the metal work function has a dramatic effect on $R_0$ for the monothiol oligoacene junctions; $R_0$ decreases by 3 orders of magnitude for a ∼1.4 eV increase in metal work function. For dithiols, the effect is not as strong ($R_0$ decreases by about a factor of 10 or 20 over the same range of work functions), but the low $R_0$ for dithiols is consistent with previous reports that chemical contacts are better for transport than physical contacts.[2,7,9,16,18]

We emphasize that the dependences of $R_0$ and $\beta$ on $\Phi$ are *completely different* (compare parts A and B of Figure 8); this is a key result. The fact that the dependences are so different implies that the two parameters are sensitive to different aspects of the junction tunneling barrier. Any model for junction transport must take this into account.

To clarify the origin of the strong dependence of $R_0$ on $\Phi$, we have also examined the correlation of $R_0$ with $\Delta\Phi$, Figure 9. Figure 9 reveals that $R_0$ correlates very well with $\Delta\Phi$ ($R^2 = 0.9$), which is not unexpected because $\Delta\Phi$ and $\Phi$ are well-correlated as shown in Figure 5C. Like the dependence of $\beta$ and $R_0$ on $\Phi$, we believe the $R_0-\Delta\Phi$ correlation is an important discovery for the overall picture of transport in these junctions, as elaborated in the next section. In addition, we have found that $R_0$ is *not* well correlated with $E_F - E_{HOMO}$ (data shown in Figure S6, Supporting Information), which can be anticipated because $E_F$ is weakly pinned in these systems, as already discussed.

We have also examined the bias dependence of $\beta$ and $R_0$ in Au−molecule−Au junctions (Figure 8C and 8D). At all biases, both $\beta$ and $R_0$ values for dithiol junctions are lower than those of monothiol junctions. However, $\beta$ and $R_0$ show little voltage dependence for dithiol junctions. In contrast, the monothiol junctions do exhibit voltage dependence for $\beta$ and $R_0$ at higher biases. In monothiol junctions, we found that $R_0$ decreased by a factor of 2 over 0−1 V while $\beta$ remained initially constant but decreased for biases greater than ±0.6 V. The changes in $\beta$ and

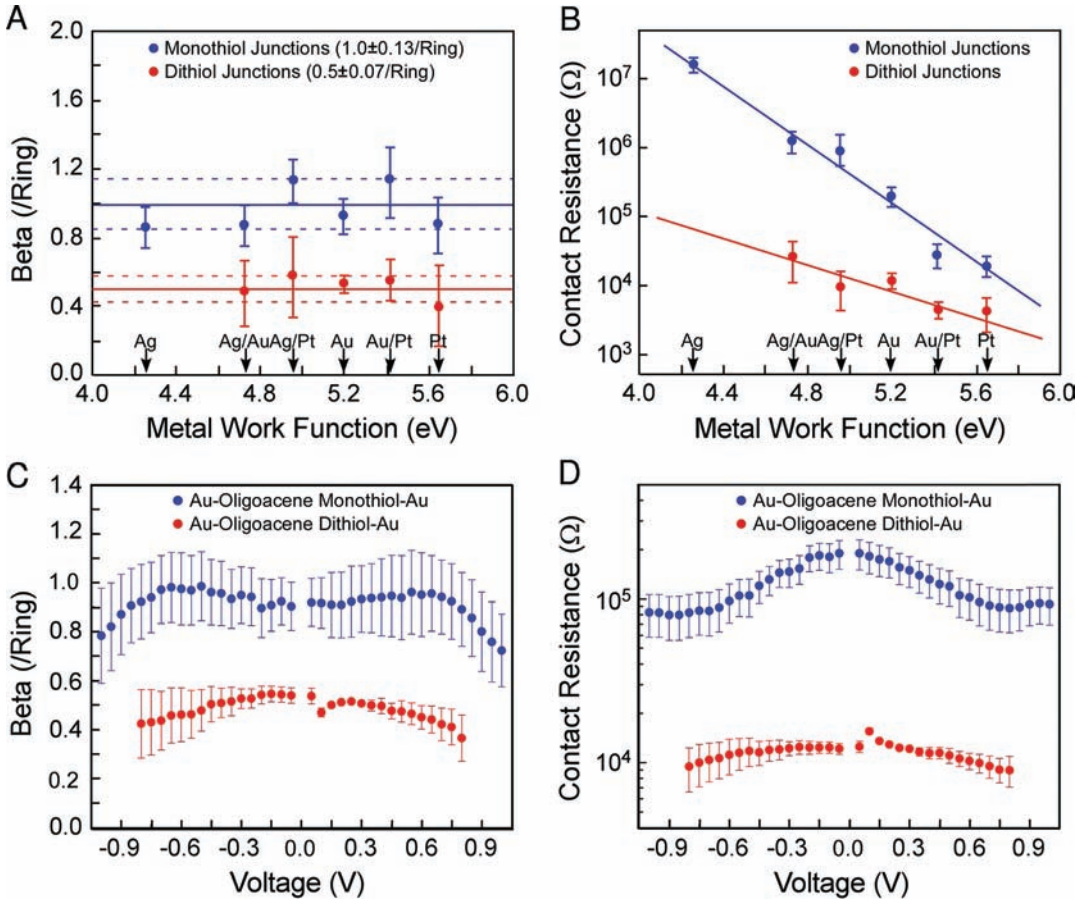


**Figure 8.** (A) $\beta$ as a function of electrode metal work function for junctions composed of oligoacene thiols and dithiols. For both thiols and dithiols, $\beta$ values appear independent of metal work function $\Phi$. The solid line is the average of each series, and dotted lines are one standard deviation above and below the average. (B) Semilog plot of contact resistance as a function of electrode metal work function $\Phi$ for junctions composed of oligoacene monothiol and dithiols. The solid lines are guides for the eye. (C, D) Dependence of $\beta$ (C) and contact resistance (D) on applied voltage in Au−oligoacene thiol−Au and Au−oligoacene dithiol−Au junctions.

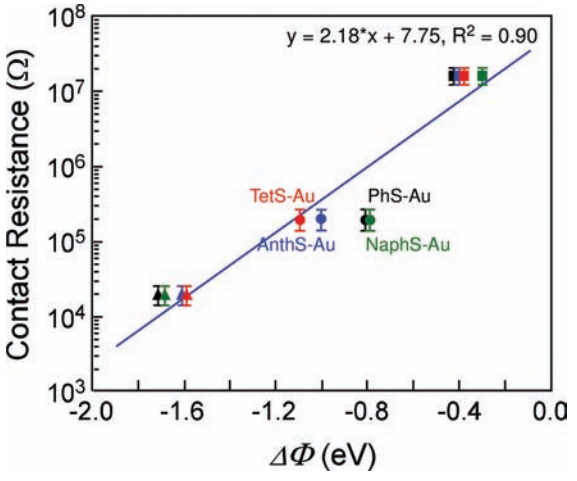


**Figure 9.** Semilog plot of contact resistance of homometal junctions versus work function change ($\Delta\Phi$). Symbols for metals: Ag (square), Au (circle), and Pt (triangle). Colors for molecules: PhSH (black), NaphSH (green), AnthSH (blue), and TetSH (red). Blue line shows a linear least-squares fit.

$R_0$ were not dramatic (certainly in the case of $R_0$, the $\Phi$ (and $\Delta\Phi$) dependence is much greater), but at least in the case of monothiols it is clear that $\beta$ does have some voltage dependence, as expected (the tunneling barrier decreases with applied bias).

**The Nature of the Tunneling Barrier.** From the above discussion, we have seen that $\beta$ for oligoacene thiols and dithiols is independent of the metal work function, which is consistent with the observation that $E_F - E_{HOMO}$ (that is the tunneling barrier through the backbone) is weakly pinned. On the other hand, $R_0$ strongly depends on $\Phi$ and more particularly on $\Delta\Phi$, which is related to the presence of metal−S bond dipoles at the contacts. To rationalize these collective observations, we propose a triple barrier model for the junction, Figure 10. The model follows the work of Heimel et al.[25,26] and is similar to the triple rectangular barriers proposed by Lee et al.,[16,17] based on similar length-dependent measurements on alkane thiols. The model explicitly addresses electrostatic potential barriers across the metal−molecule−metal junction. Figure 10A, for example, depicts the electrostatic potential profile across an Ag−S-molecule interface, which is a result of combining the potentials for the metal, molecule, and the Ag−S bond dipole (BD). *It is the magnitude of the BD that changes for junctions based on Ag, Au, or Pt (panels A, B, and C).* The changing BD results in different "chemical contact barriers" as shown. Panel D represents the full triple barriers (left contact−bridge−right contact) for thiol and dithiol junctions. The heights of the contact barriers are

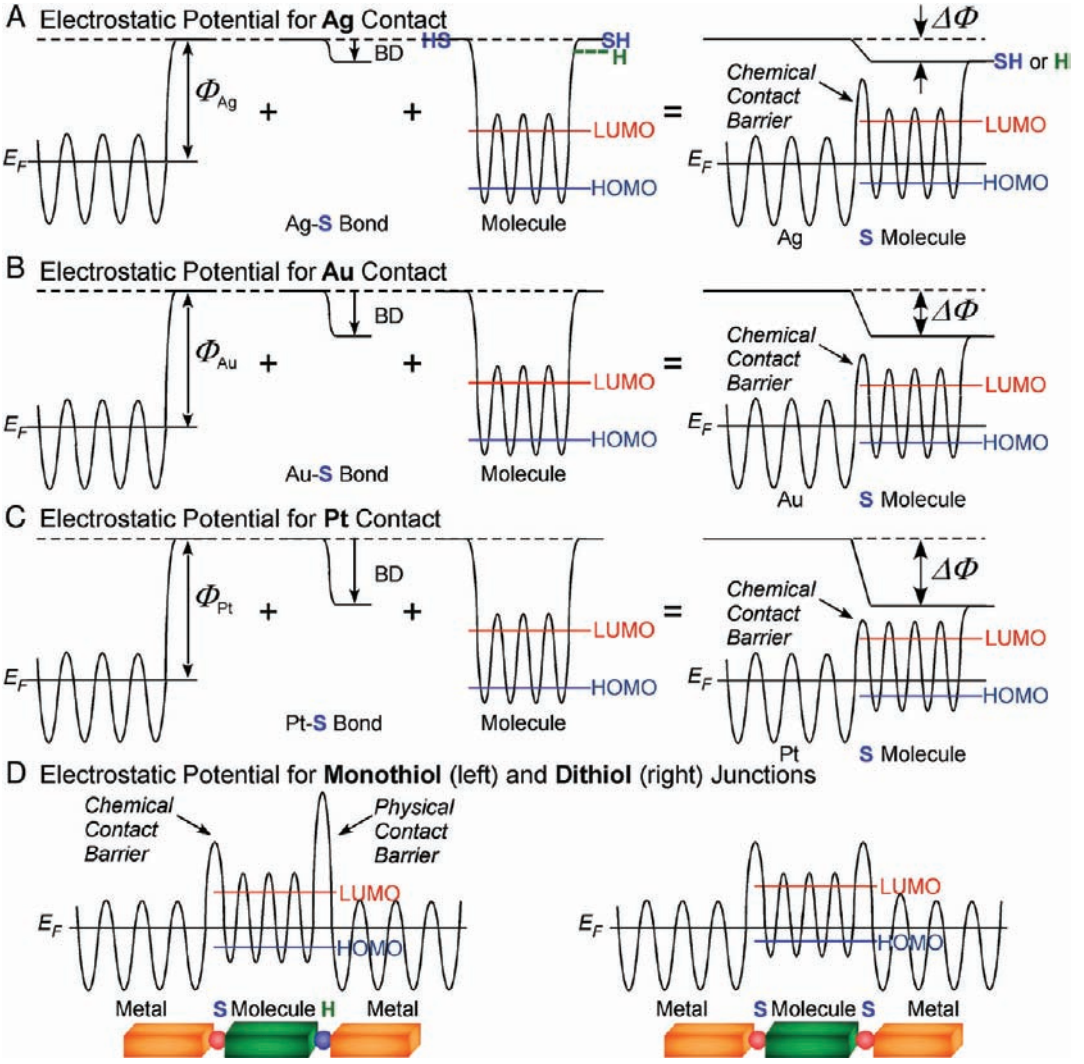


**Figure 10.** Schematic diagram showing electrostatic potential change at the molecule−metal interfaces and resulting molecular energy level alignment as well as the formation of contact barriers depending on metal substrates for (A) Ag, (B) Au, and (C) Pt contacts. Panel D shows schematic tunneling barriers formed at the metal−oligoacene monothiol−metal (left) and metal−oligoacene dithiol−metal junctions (right).

proportional to $\Delta\Phi$, and, as we have shown, the absolute value of $\Delta\Phi$ becomes larger as the bare metal work function increases, Figure 5C.

We propose that large contact barriers give rise to large $R_0$ values. Likewise, we propose that weak pinning of the HOMO position, due to the BD formation, leads to the independence of $\beta$ on $\Phi$. The precise value of $E_F - E_{HOMO}$ will depend strongly on the number of chemical contacts (1 versus 2) and thus $\beta$ will be smaller for dithiols versus monothiols (Figure 10D). Theoretical calculations by Bredas and Ratner also support similar HOMO band alignments on different metal substrates, and they attribute conductance differences of junctions mainly to electronic coupling at the interfaces.[24,25] Overall, the qualitative description of the junction electrostatics presented in Figure 10 is consistent with our quantitative measurements (it provides a basis for understanding the very different dependences of $\beta$ and $R_0$ on $\Phi$), and thus we believe it may provide valuable physical insight into the properties of molecular tunnel junctions. We reiterate that motivation for the triple barrier model came from the very different dependences of $\beta$ and $R_0$ on $\Phi$.

**Transport at Higher Bias.** The discussion so far has focused on junction resistance data at low biases. With increasing voltages, there is a steeper dependence of $I$ on $V$, as expected.[14,27,28,45,64,66−68] Figure 11 displays log−log plots of the $I-V$ characteristics for PhSH, NaphSH, AnthSH, $Ph(SH)_2$, $Naph(SH)_2$, and $Anth(SH)_2$ with Au contacts. The vertical dotted lines correspond to the voltages ($V_{trans}$) where there is a change in the slopes of the plots. For convenience only (not theoretically motivated), the currents were fit to a power law, $I \propto V^n$; the values of $n$ are indicated in Figure 11. Below $V_{trans}$ for both monothiol and dithiol junctions, $I$ depends approximately linearly on $V$ ($n$ = 1.1−1.4), as expected for low bias nonresonant tunneling. Above $V_{trans}$, $n$ is 2.1−4.6. Basic theories of tunneling of course predict strong increases in current as the applied potential becomes comparable to the average tunneling barrier,[56] and qualitatively $V_{trans}$ should be a measure of when this occurs.

Figure 12 summarizes the dependence of $V_{trans}$ for monothiol junctions on the metal work function, molecular length, and HOMO level position. Similar data for dithiols are shown in Figure S8. From Figure 12A, it is clear $V_{trans}$ decreases systematically with both increasing metal work function and increasing molecular length. The work function dependence of $V_{trans}$ is relatively weak,

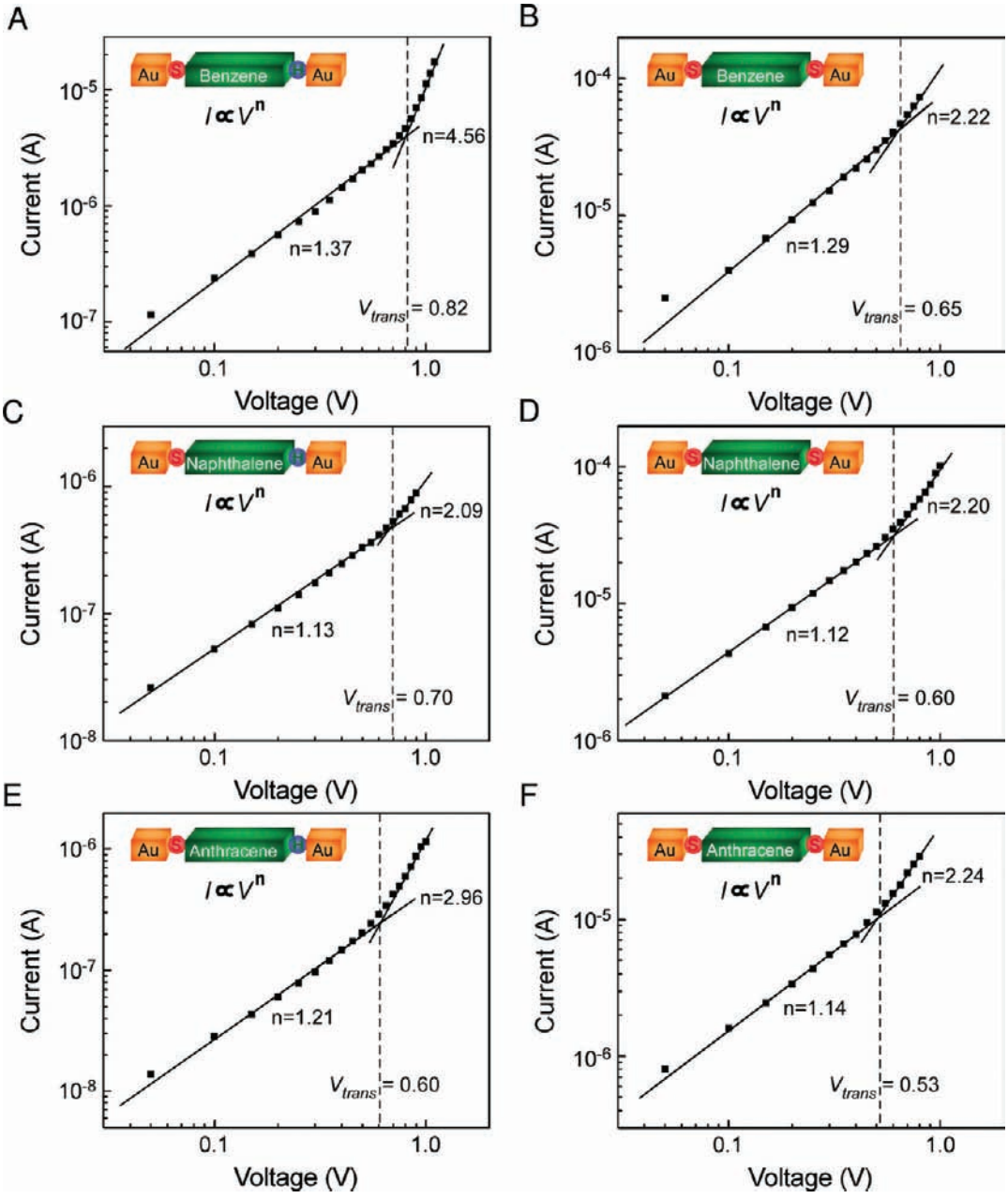


**Figure 11.** Log−log plot of representative Au−molecule−Au junctions: (A) Au−benzene thiol−Au, (B) Au−benzene dithiol−Au, (C) Au−naphthalene thiol−Au, (D) Au−naphthalene dithiol−Au, (E) Au−anthracene thiol−Au, and (F) Au−anthracene dithiol−Au. The dotted line corresponds to the voltage ($V_{trans}$) where the current−voltage relationship becomes steeper. The slopes in the log−log plots are from the equation, $I \propto V^n$.

i.e., a 1.3 eV change in the work function results in only ~0.2 eV change in $V_{trans}$. However, $V_{trans}$ is more sensitive to molecular length, suggesting that there is a dependence on the HOMO level offset. Figure 12B shows the dependence of $V_{trans}$ on $E_F - E_{HOMO}$, which is the most striking result; the correlation is excellent ($R^2$ = 0.92) and reveals that $V_{trans}$ increases linearly with $E_F - E_{HOMO}$ as we and others have reported before for similar systems.[14,27,28,45,64,66,67,68] In addition, for a given set of electrodes, $V_{trans}$ is lower for dithiol junctions compared to the corresponding monothiol junctions (see Figure 11). Thus, $V_{trans}$ depends on all the critical variables in this study: molecular length, type of contact, and metal work function.

The meaning of $V_{trans}$ is currently being debated in the literature.[27,28,55,64,66−73] Originally, we and our collaborators identified $V_{trans}$ as the minimum in a Fowler−Nordheim plot ($\ln(I/V^2)$ versus $1/V$) and suggested that $V_{trans}$ corresponded to the onset of field emission in the junction.[27,28] This idea was motivated by (1) the observation that for voltages above $V_{trans}$ the Fowler−Nordheim plot exhibited approximately linear behavior with a negative slope, as expected for field emission, (2) the clear correlation of $V_{trans}$ with $E_F - E_{HOMO}$, and (3) the fact that fields in molecular junctions range from $10^8$ to $10^9$ V/m. However, the field emission interpretation has been called into question. Huisman et al. pointed out that within the simple

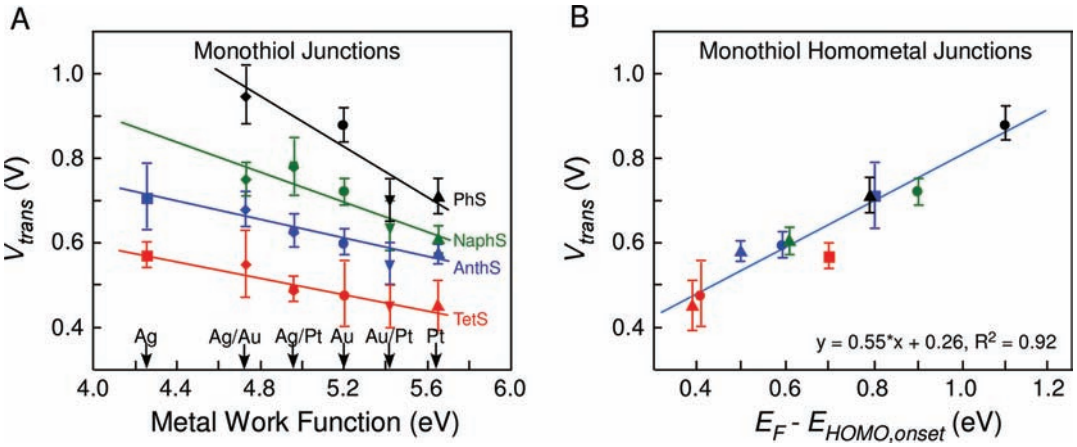


**Figure 12.** (A) $V_{trans}$ as a function of electrode work function for junctions composed of oligoacene monothiols. (B) $V_{trans}$ as a function of $E_F - E_{HOMO,onset}$ for homometal junctions composed of oligoacene monothiols. Symbols for metals: Ag (square), Au (circle), Pt (triangle), Ag/Au (diamond), Ag/Pt (pentagon), and Au/Pt (inverted triangle). Colors for molecules: PhSH (black), NaphSH (green), AnthSH (blue), and TetSH (red).

Simmons barrier model for the junction that $V_{trans}$ should scale with $(E_F - E_{HOMO})^{1/2}$, not $E_F - E_{HOMO}$.[64] Furthermore, modeling the junction $I-V$ characteristics with the Landauer equation and a broadened molecular state also yielded the minimum in a Fowler–Nordheim plot; the concept of field emission was not necessary.

The question remains as to what occurs at $V_{trans}$, for example whether at this voltage some of the tail states in the junction electronic density of states become accessible for resonant tunneling.[71] One would expect that in such a situation, $\beta$ would depend more strongly on voltage than what we observe. The contacts also have an important effect on the value of $V_{trans}$,[68,69] and it may be difficult to develop a model without knowing how potential varies across a junction (i.e., how the voltage drops at the contacts versus across the molecular backbone). Precise understanding of $V_{trans}$ and its relation to the contact barriers and the electronic states in the junction will require further experimental and theoretical work. However, the data in Figures 11 and 12 add to the growing body of experimental results in the literature[27,28,66–73] that show $V_{trans}$ is a reproducible quantity that is directly related to the HOMO (or LUMO) position in the junction.

## SUMMARY

We investigated the transport properties of tunnel junctions based on rigid, conjugated oligoacene monothiols and dithiols as a function of molecular length and contact work function and correlated the results with electronic structure determined by UPS. UPS revealed weak Fermi level pinning in this system which was associated with the formation of strong metal–S bond dipoles. Length-dependent transport measurements showed the junction resistance was strongly affected by the surface linker types (chemical/physical vs bichemical contact). The tunneling attenuation factor, $\beta$, was 1.0 per ring or 0.5/Å for the monothiol series and 0.5 per ring or 0.2/Å for the dithiol series, and contact resistance, $R_0$, was 10–100 times lower for dithiol junctions, indicating that chemical contacts reduce both the tunneling barrier height *and* contact resistance significantly. When combinations of metals (Ag, Au, and Pt) were employed as electrodes in the junctions, $\beta$ values were independent of metal work function, within error, while $R_0$ exhibited strong work function dependence and was significantly reduced as work function increased. This behavior was self-consistently explained in terms of the contact bond dipoles and the electronic structure of the junction; namely $\beta$ is independent of contact type because of weak Fermi level pinning ($E_F - E_{HOMO}$ varies only weakly with $\Phi$), but $R_0$ varies strongly with contact type because of the metal–S bond dipole that is responsible for the Fermi level pinning. A previously published triple barrier model for molecular junctions was proposed to rationalize these results in which contact barriers, proportional to the size of the interfacial bond dipoles, determine $R_0$, and the bridge barrier, $E_F - E_{HOMO}$, determines $\beta$. Finally, for larger voltage sweeps, a characteristic transition voltage $V_{trans}$ associated with steeper dependence of current on voltage was identified. $V_{trans}$ values were well correlated with $E_F - E_{HOMO}$. Overall, the results presented here provide a comprehensive data set for tunneling through the oligoacene systems. We believe the findings on the oligoacene model system will be broadly representative of the behavior of other junctions based on $\pi$-conjugated molecules sandwiched between metal contacts. In particular, we expect that other systems will show that $R_0$ and $\beta$ are sensitive to different parts of the junction tunneling barrier.

## ASSOCIATED CONTENT

**Supporting Information.** Monolayer characterization details, UV–visible absorption spectra, transmission analysis, correlation between $V_{trans}$ and the metal work function for oligoacene dithiol junctions. This material is available free of charge via the Internet at http://pubs.acs.org.

## AUTHOR INFORMATION

**Corresponding Author**
frisbie@umn.edu

## ACKNOWLEDGMENT

This article is dedicated to Dr. Seong Ho Choi, colleague, co-author, and friend, whose untimely death in December 2010 was a great loss for us. C.D.F. and X.Y.Z. thank the National Science Foundation (CHE-0616427) for financial support. C.D.F. also thanks NSF for a Special Creativity Award. B.S.K.

thanks Professor Thomas R. Hoye for help and discussion on molecular synthesis. Parts of this work were carried out in the College of Science and Engineering Characterization Facility, University of Minnesota, which receives partial support from NSF through the NNIN program.

## REFERENCES


(1) Lindsay, S. M.; Ratner, M. A. *Adv. Mater.* **2007**, *19*, 23.
(2) Kushmerick, J. G. *Mater. Today* **2005**, *8*, 26.
(3) Chen, F.; Hihath, J.; Huang, Z. F.; Li, X. L.; Tao, N. J. *Annu. Rev. Phys. Chem.* **2007**, *58*, 535.
(4) McCreery, R. L.; Bergren, A. J. *Adv. Mater.* **2009**, *21*, 4303.
(5) Park, Y. S.; Whalley, A. C.; Kamenetska, M.; Steigerwald, M. L.; Hybertsen, M. S.; Nuckolls, C.; Venkataraman, L. *J. Am. Chem. Soc.* **2007**, *129*, 15768.
(6) Ko, C.-H.; Huang, M.-J.; Fu, M.-D.; Chen, C.-H. *J. Am. Chem. Soc.* **2009**, *132*, 756.
(7) Engelkes, V. B.; Beebe, J. M.; Frisbie, C. D. *J. Am. Chem. Soc.* **2004**, *126*, 14287.
(8) Kim, B.-S.; Beebe, J. M.; Jun, Y.; Zhu, X.-Y.; Frisbie, C. D. *J. Am. Chem. Soc.* **2006**, *128*, 4970.
(9) Wu, S. M.; Gonzalez, M. T.; Huber, R.; Grunder, S.; Mayor, M.; Schonenberger, C.; Calame, M. *Nat. Nanotechnol.* **2008**, *3*, 569.
(10) Malen, J. A.; Doak, P.; Baheti, K.; Tilley, T. D.; Segalman, R. A.; Majumdar, A. *Nano Lett.* **2009**, *9*, 1164.
(11) Kamenetska, M.; Quek, S. Y.; Whalley, A. C.; Steigerwald, M. L.; Choi, H. J.; Louie, S. G.; Nuckolls, C.; Hybertsen, M. S.; Neaton, J. B.; Venkataraman, L. *J. Am. Chem. Soc.* **2010**, *132*, 6817.
(12) Park, Y. S.; Widawsky, J. R.; Kamenetska, M.; Steigerwald, M. L.; Hybertsen, M. S.; Nuckolls, C.; Venkataraman, L. *J. Am. Chem. Soc.* **2009**, *131*, 10820.
(13) Beebe, J. M.; Engelkes, V. B.; Miller, L. L.; Frisbie, C. D. *J. Am. Chem. Soc.* **2002**, *124*, 11268.
(14) Choi, S. H.; Kim, B.; Frisbie, C. D. *Science* **2008**, *320*, 1482.
(15) Lu, Q.; Liu, K.; Zhang, H.; Du, Z.; Wang, X.; Wang, F. *ACS Nano* **2009**, *3*, 3861 .
(16) Wang, G.; Kim, T. W.; Jang, Y. H.; Lee, T. *J. Phys. Chem. C* **2008**, *112*, 13010.
(17) Wang, G.; Kim, T. W.; Lee, H.; Lee, T. *Phys. Rev. B* **2007**, *76*, 205320.
(18) Liu, K.; Li, G. R.; Wang, X. H.; Wang, F. S. *J. Phys. Chem. C* **2008**, *112*, 4342.
(19) Note that according to eq 1, $R$ is proportional to $R_0$ at any molecular length $s$, which is very different from the situation in macroscopic transport measurements on semiconductors. In those cases, $R_0$ is normally an additive factor to the total $R$ and becomes less important as the contacts become further apart. Equation 1 shows that because $R_0$ is a multiplicative coefficient it is important at any length $s$. See also refs 7 and 57.
(20) Dameron, A. A.; Ciszek, J. W.; Tour, J. M.; Weiss, P. S. *J. Phys. Chem. B* **2004**, *108*, 16761.
(21) Quinn, J. R.; Foss, F. W.; Venkataraman, L.; Breslow, R. *J. Am. Chem. Soc.* **2007**, *129*, 12376.
(22) McCreery, R. *Electrochem. Soc. Interface* **2004**, *13*, 46.
(23) Kiguchi, M.; Miura, S.; Hara, K.; Sawamura, M.; Murakoshi, K. *Appl. Phys. Lett.* **2007**, *91*, 053110.
(24) Yaliraki, S. N.; Kemp, M.; Ratner, M. A. *J. Am. Chem. Soc.* **1999**, *121*, 3428.
(25) Heimel, G.; Romaner, L.; Zojer, E.; Bredas, J. L. *Nano Lett.* **2007**, *7*, 932.
(26) Heimel, G.; Romaner, L.; Bredas, J. L.; Zojer, E. *Phys. Rev. Lett.* **2006**, *96*, 196806.
(27) Beebe, J. M.; Kim, B.-S.; Frisbie, C. D.; Kushmerick, J. G. *ACS Nano* **2008**, *2*, 827.
(28) Beebe, J. M.; Kim, B.-S.; Gadzuk, J. W.; Frisbie, C. D.; Kushmerick, J. G. *Phys. Rev. Lett.* **2006**, *97*, 026801.
(29) Xue, Y. Q.; Datta, S.; Ratner, M. A. *J. Chem. Phys.* **2001**, *115*, 4292.
(30) Xue, Y. Q.; Ratner, M. A. *Phys. Rev. B* **2004**, *69*, 085403.
(31) Reddy, P.; Jang, S. Y.; Segalman, R. A.; Majumdar, A. *Science* **2007**, *315*, 1568.
(32) Armarego, W. L. F.; Chai, C. L. L. *Purification of Laboratory Chemicals*, 5th ed.; Butterworth Heinemann: Boston, 2003.
(33) Shaporenko, A.; Elbing, M.; Baszczyk, A.; von Hanisch, C.; Mayor, M.; Zharnikov, M. *J. Phys. Chem. B* **2006**, *110*, 4307.
(34) Ulman, A. *Chem. Rev.* **1996**, *96*, 1533.
(35) Li, Z. Y.; Chang, S. C.; Williams, R. S. *Langmuir* **2003**, *19*, 6744.
(36) Engelkes, V. B.; Beebe, J. M.; Frisbie, C. D. *J. Phys. Chem. B* **2005**, *109*, 16801.
(37) Salomon, A.; Cahen, D.; Lindsay, S.; Tomfohr, J.; Engelkes, V. B.; Frisbie, C. D. *Adv. Mater.* **2003**, *15*, 1881.
(38) Zangmeister, C. D.; Picraux, L. B.; van Zee, R. D.; Yao, Y. X.; Tour, J. M. *Chem. Phys. Lett.* **2007**, *442*, 390.
(39) Zangmeister, C. D.; Robey, S. W.; van Zee, R. D.; Yao, Y.; Tour, J. M. *J. Phys. Chem. B* **2004**, *108*, 16187.
(40) Alloway, D. M.; Hofmann, M.; Smith, D. L.; Gruhn, N. E.; Graham, A. L.; Colorado, R.; Wysocki, V. H.; Lee, T. R.; Lee, P. A.; Armstrong, N. R. *J. Phys. Chem. B* **2003**, *107*, 11690.
(41) Campbell, I. H.; Rubin, S.; Zawodzinski, T. A.; Kress, J. D.; Martin, R. L.; Smith, D. L.; Barashkov, N. N.; Ferraris, J. P. *Phys. Rev. B* **1996**, *54*, R14321.
(42) Bilic, A.; Reimers, J. R.; Hush, N. S. *J. Chem. Phys.* **2005**, *122*, 094708.
(43) Romaner, L.; Heimel, G.; Zojer, E. *Phys. Rev. B* **2008**, *77*, 045113.
(44) Zangmeister, C. D.; Robey, S. W.; van Zee, R. D.; Kushmerick, J. G.; Naciri, J.; Yao, Y.; Tour, J. M.; Varughese, B.; Xu, B.; Reutt-Robey, J. E. *J. Phys. Chem. B* **2006**, *110*, 17138.
(45) Zangmeister, C. D.; Beebe, J. M.; Naciri, J.; Kushmerick, J. G.; van Zee, R. D. *Small* **2008**, *4*, 1143.
(46) Zangmeister, C. D.; Robey, S. W.; vanZee, R. D.; Yao, Y.; Tour, J. M. *J. Am. Chem. Soc.* **2004**, *126*, 3420.
(47) Heimel, G.; Romaner, L.; Bredas, J. L.; Zojer, E. *Surf. Sci.* **2006**, *600*, 4548.
(48) Heimel, G.; Romaner, L.; Bredas, J. L.; Zojer, E. *Langmuir* **2008**, *24*, 474.
(49) Kubatkin, S.; Danilov, A.; Hjort, M.; Cornil, J.; Bredas, J. L.; Stuhr-Hansen, N.; Hedegard, P.; Bjornholm, T. *Nature* **2003**, *425*, 698.
(50) Hedegard, P.; Bjornholm, T. *Chem. Phys.* **2005**, *319*, 350.
(51) Kaasbjerg, K.; Flensberg, K. *Nano Lett.* **2008**, *8*, 3809.
(52) Thygesen, K. S.; Rubio, A. *Phys. Rev. Lett.* **2009**, *102*, 046802.
(53) Garcia-Lastra, J. M.; Rostgaard, C.; Rubio, A.; Thygesen, K. S. *Phys. Rev. B* **2009**, *80*, 245427.
(54) Neaton, J. B.; Hybertsen, M. S.; Louie, S. G. *Phys. Rev. Lett.* **2006**, *97*, 216405.
(55) Chen, J. Z.; Markussen, T.; Thygesen, K. S. *Phys. Rev. B* **2010**, *82*, 121412.
(56) Simmons, J. G. *J. Appl. Phys.* **1963**, *34*, 1973.
(57) Nitzan, A. *Annu. Rev. Phys. Chem.* **2001**, *52*, 681.
(58) Beebe, J. M.; Kushmerick, J. G. *Appl. Phys. Lett.* **2007**, *90*, 083117.
(59) Terabe, K.; Hasegawa, T.; Nakayama, T.; Aono, M. *Nature* **2005**, *433*, 47.
(60) Yamada, R.; Kumazawa, H.; Noutoshi, T.; Tanaka, S.; Tada, H. *Nano Lett.* **2008**, *8*, 1237.
(61) Tada, T.; Nozaki, D.; Kondo, M.; Hamayama, S.; Yoshizawa, K. *J. Am. Chem. Soc.* **2004**, *126*, 14182.
(62) Quinn, J. R.; Foss, F. W.; Venkataraman, L.; Hybertsen, M. S.; Breslow, R. *J. Am. Chem. Soc.* **2007**, *129*, 6714.
(63) Unpublished result: We found that below a tip load of 10 nN in monothiol junctions, the $\beta$ value is almost constant while above 10 nN, the $\beta$ value is gradually decreased. Importantly, we have to increase the load to ~20 nN to get the $\beta$ value (0.5/ring) of dithiol junctions. From our experience, 20 nN is a very high load. Though the dithiol molecules

have tip adhesive forces stronger than those of monothiols, we do not believe that this can account for the lower $\beta$ value.

(64) Huisman, E. H.; Guedon, C. M.; van Wees, B. J.; van der Molen, S. J. *Nano Lett.* **2009**, *9*, 3909.

(65) It is also interesting to consider the impact of different Au−S−molecule bond angles on $R_0$. The bond angles may change systematically with electrode type, Ag, Au, Pt. We have not systematically measured bond angles here, and the degree to which bond angles versus work function play a role will need to be determined.

(66) Song, H.; Kim, Y.; Jang, Y. H.; Jeong, H.; Reed, M. A.; Lee, T. *Nature* **2009**, *462*, 1039.

(67) Wang, G.; Kim, T. W.; Jo, G.; Lee, T. *J. Am. Chem. Soc.* **2009**, *131*, 5980.

(68) Pakoulev, A. V.; Burtman, V. *J. Phys. Chem. C* **2009**, *113*, 21413.

(69) Yu, L. H.; Gergel-Hackett, N.; Zangmeister, C. D.; Hacker, C. A.; Richter, C. A.; Kushmerick, J. G. *J. Phys.: Condens. Matter* **2008**, *20*, 374114.

(70) Malen, J. A.; Doak, P.; Baheti, K.; Tilley, T. D.; Majumdar, A.; Segalman, R. A. *Nano Lett.* **2009**, *9*, 3406.

(71) Araidai, M.; Tsukada, M. *Phys. Rev. B* **2010**, *81*, No. 235114.

(72) Bennett, N.; Xu, G.; Esdaile, L. J.; Anderson, H. L.; Macdonald, J. E.; Elliott, M. *Small* **2010**, *6*, 2604.

(73) Baldea, I. *Chem. Phys.* **2010**, *377*, 15.